LETTER

Pinning of diffusional patterns by non-uniform curvature

A Letters Journal Exploring the Frontiers of Physics

August 2019

EPL, **127** (2019) 48001 www.epljournal.org
doi: 10.1209/0295-5075/127/48001

Pinning of diffusional patterns by non-uniform curvature

John R. Frank[1], Jemal Guven[2], Mehran Kardar[1] and Henry Shackleton[3]

[1] *Department of Physics, Massachusetts Institute of Technology - Cambridge, MA 02138, USA*
[2] *Instituto de Ciencias Nucleares, Universidad Nacional Autónoma de México - Apdo. Postal 70-543, 04510 México, DF, Mexico*
[3] *Department of Physics, Harvard University - Cambridge, MA 02138, USA*

received 5 June 2019; accepted in final form 10 August 2019
published online 9 September 2019

PACS 82.40.Ck – Pattern formation in reactions with diffusion, flow, and heat transfer
PACS 89.75.Kd – Patterns
PACS 02.40.Ky – Riemannian geometries

Abstract – Diffusion-driven patterns appear on curved surfaces in many settings, initiated by unstable modes of an underlying Laplacian operator. On a flat surface or perfect sphere, the patterns are degenerate, reflecting translational/rotational symmetry. Deformations, *e.g.*, by a bulge or indentation, break symmetry and can pin a pattern. We adapt methods of conformal mapping and perturbation theory to examine how curvature inhomogeneities select and pin patterns, and confirm the results numerically. The theory provides an analogy to quantum mechanics in a geometry-dependent potential and yields intuitive implications for cell membranes, tissues, thin films, and noise-induced quasipatterns.

In 1952, Turing coined the term "morphogen" in a seminal paper that showed how combining diffusion with generalized reactions can create spatial and temporal patterns even though separately each leads to uniform, static concentrations [1]. Such reaction-diffusion (RD) patterns are but one example of diffusion-driven instabilities that have since been studied on scales ranging from microns in cells [2] and active fluids [3–8], millimeters in hydrodynamics [9], centimeters in zoology [10], to meters in ecology [11]. Diffusion-driven patterns are known to determine morphology [12] in model organisms like zebrafish [13,14] and complex organs like the eye [15]. Recent theoretical progress in patterning [16,17] encourages further study.

Substrate curvature plays a role in pattern formation in many systems, including cell membranes [18] and thin films [19]. The importance of surface curvature on collective behavior has recently been explored in liquid crystals [20], flocking [21], and wave propagation [22]. Closer to our work, the geometric dependence of pattern formation has recently been studied in various models of protein [23,24] and molecular bonding [25].

Recent studies of Turing patterns have explored the effects of curvature on highly symmetric shapes such as spheres, cylinders, toroids [26,27], and ellipsoids [28] where the Laplacian is known in closed form. Inhomogeneities in curvature, such as protrusions or cavities, reduce such symmetries and can pin or modify the patterns. To understand how nonuniform curvature can entrain and modify patterns, we study perturbations to the Laplacian, and its eigenmodes. To our knowledge, the intimate link between pinning of patterns and the spectrum of the Laplacian has not been pursued.

We follow a two-prong strategy. First, we identify the *onset* of instabilities, by linearizing evolution equations expressed in terms of the appropriate "modes", *e.g.*, Fourier, cylindrical, or spherical harmonics. Modes with the largest positive real part grow fastest and are harbingers of the final patterns molded by nonlinearities. The modes are eigenfunctions of the diffusion (Laplacian) operator on the relevant manifold. Symmetries of the manifold, reflected in degeneracies of the eigenfunctions, must be broken in the final patterns. Previous work on the Laplacian on Riemannian manifolds focused on its determinant [29–32] and short-time behavior appropriate to field theory [33–35]. We focus instead on how nonuniform curvature breaks degeneracies, pinning eigenfunctions to inhomogeneities. To do this, we utilize conformal mappings and perturbation theory. There is no guarantee, however, that patterns resulting from nonlinear evolution are similarly entrained, so the second step in our study explores patterns with simulations. We implemented the Thomas-Murray RD equations [10] on COMSOL Multiphysics® [36]. We conclude with suggestions for experiments.

We first consider a cylinder with axially symmetric deformations described in cylindrical polar coordinates as $\rho = R(z)$. The surface line element is

$$\mathrm{d}s^2 = (1 + R_z^2)\mathrm{d}z^2 + R^2\mathrm{d}\varphi^2\,, \tag{1}$$

where R_z denotes the derivative with respect to z. The Laplacian of a scalar ϕ is

$$\Delta\phi = \frac{1}{\sqrt{g}}\partial_a(\sqrt{g}g^{ab}\partial_b\phi), \tag{2}$$

where g_{ab} is the metric of the underlying geometry; g is the determinant of the metric. Conformal mapping simplifies analysis through mapping to a flat geometry. We introduce a conformal axial coordinate v, such that the line element acquires the conformally flat form

$$\mathrm{d}s^2 = \Omega^2(v)(\mathrm{d}v^2 + R_0^2\mathrm{d}\varphi^2), \tag{3}$$

where R_0 is the asymptotic radius and Ω is the conformal factor. In the conformal coordinates, $\sqrt{g} = \Omega^2 R_0$, and thus the Laplacian on the deformed geometry takes the simple form $\Delta^G = \Omega^{-2}\Delta^0$, where Δ^0 is the Laplacian in the conformally flat coordinates. Since the behavior of Δ^0 is well understood, and Ω is determined by the equality of eqs. (1) and (3), this conformal mapping provides a tractable method of understanding Δ^G.

Solutions for v and Ω for arbitrary $R(z)$ are in the supplementary material `Supplementarymaterial.pdf` (SM). To develop the perturbation theory, we set $R = R_0(1 + \epsilon h(z))$, in which case $v \approx z$ and $\Omega \approx 1 + 2\epsilon h(v)$ to lowest order. Therefore, the eigenfunctions ϕ_k of Δ^G with eigenvalues λ, satisfy

$$-\Delta^0\phi_k + 2\epsilon\lambda\epsilon h(v)\phi_k = -\lambda\phi_k + \mathcal{O}(\epsilon^2). \tag{4}$$

In analogy with quantum mechanics, one can interpret the deformation as giving rise to a potential in the conformal coordinates, whose magnitude is dependent on the eigenvalue λ. (This differs from da Costa's geometric potential, which comes from confining a particle to a surface [37].) For physical phenomena described by the Laplacian, this mapping can be interpreted as the replacement of the diffusion operator $-D\Delta$ on a deformed geometry, with a spatially dependent diffusion coefficient $\tilde{D}(v) \equiv D/\Omega^2$ in the conformally related homogeneous geometry. This provides an intuitive picture of how diffusion is modified by curvature.

The undistorted cylinder of length L with periodic boundary conditions has eigenfunctions and eigenvalues

$$\begin{aligned}\phi_{sk}^{(0)} &= \frac{e^{is\varphi}}{\sqrt{2\pi R_0}}\frac{e^{i2\pi kz/L}}{\sqrt{L}},\\ \lambda_{sk}^{(0)} &= -\frac{s^2}{R_0^2} - \left(\frac{2\pi k}{L}\right)^2 \equiv -\bar{s}^2 - \bar{k}^2,\end{aligned}$$

with integers s and k. Consider an axially symmetric bump on the cylinder, shaped like a Gaussian of standard deviation σ and height v_0. We apply the Rayleigh-Schrödinger perturbation theory to eq. (4) to calculate eigenvalue corrections to first order in $\epsilon \equiv v_0/R$, which simplify for the case $s = 0$ to

$$\lambda_{0k}^{\pm} = -\bar{k}^2\left(1 \pm \frac{2\epsilon\sigma\sqrt{2\pi}}{L}e^{-2\bar{k}^2\sigma^2}\right) + \mathcal{O}(\epsilon^2).$$

The positive/negative sign is set by the mode: positive for cosine (symmetric) modes, and negative for sine (antisymmetric) modes. The sign of ϵ depends on the orientation of the ridge-like deformation: positive for a bulge and negative for a constriction. Thus, to first order, a ridge breaks the degeneracy in the eigenvalues of a Laplacian on the cylinder, causing the eigenvalues of sine (cosine) modes to become more negative in the case of an outward (inward) ridge. This correction is largest for $2\pi/\bar{k} = 4\pi\sigma$, when the wavelength is approximately twice the width of the ridge. This is a general trait of deformations, explored later for a rippled cylinder. The ridge can be positioned anywhere along the cylinder, and the modes will shift with the ridge.

Modifications to the Laplacian spectrum affect any physical system involving diffusion. For example, consider a two-component RD system:

$$\partial_t\begin{pmatrix}\Psi_1(\mathbf{x},t)\\ \Psi_2(\mathbf{x},t)\end{pmatrix} = \overbrace{\begin{pmatrix}R_1\left(\Psi_1,\Psi_2\right)\\ R_2\left(\Psi_1,\Psi_2\right)\end{pmatrix}}^{\text{Reactions}} + \overbrace{\begin{pmatrix}\nu_1 & 0\\ 0 & \nu_2\end{pmatrix}\Delta^G\begin{pmatrix}\Psi_1\\ \Psi_2\end{pmatrix}}^{\text{Diffusion}}. \tag{5}$$

After linearization, small deviations around a uniform stable fixed point of the reactions, $(\Psi_1,\Psi_2)^*$, evolve as

$$\begin{pmatrix}\Psi_1(\mathbf{x},t)\\ \Psi_2(\mathbf{x},t)\end{pmatrix} = \begin{pmatrix}\Psi_1\\ \Psi_2\end{pmatrix}^* + \sum_k\begin{pmatrix}u_{1k}\\ u_{2k}\end{pmatrix}e^{t\omega(k)}\phi_k\left(\mathbf{x}\right),$$

with $\omega(k)$ satisfying the eigenvalue equation, $\mathbf{M}(\lambda) = \mathbf{R} + \lambda\boldsymbol{\nu}$,

$$\left[\begin{pmatrix}R_{1,1} & R_{1,2}\\ R_{2,1} & R_{2,2}\end{pmatrix}^* + \begin{pmatrix}\nu_1\lambda_k & 0\\ 0 & \nu_2\lambda_k\end{pmatrix}\right]\begin{pmatrix}u_{1k}\\ u_{2k}\end{pmatrix} = \omega(k)\begin{pmatrix}u_{1k}\\ u_{2k}\end{pmatrix}.$$

While the diffusion and stable reaction matrices separately possess negative eigenvalues, Turing showed that their sum can have positive eigenvalues ($\omega_+(k) > 0$) signaling finite-wavelength instabilities [1]. The possibly degenerate modes, k^*, with largest eigenvalue evolve to the final pattern. On a cylinder with a ridge, the degeneracy between sine and cosine modes is broken: an outward (inward) ridge leads to sine (cosine) growing faster.

This linear analysis indicates only the onset of instabilities. To understand the patterns formed after nonlinearities stabilize the dynamics, we conducted finite element simulations of the Thomas-Murray model [10]:

$$\begin{aligned}\dot{\Psi}_1 &= \nu_1\Delta^G\Psi_1 + \gamma\left(\Psi_1 - u_{10} - \tfrac{\rho\Psi_1\Psi_2}{1+\Psi_1+\Psi_1^2/K}\right),\\ \dot{\Psi}_2 &= \nu_2\Delta^G\Psi_2 + \gamma\left(\alpha\left(\Psi_2 - u_{20}\right) - \tfrac{\rho\Psi_1\Psi_2}{1+\Psi_1+\Psi_1^2/K}\right).\end{aligned} \tag{6}$$

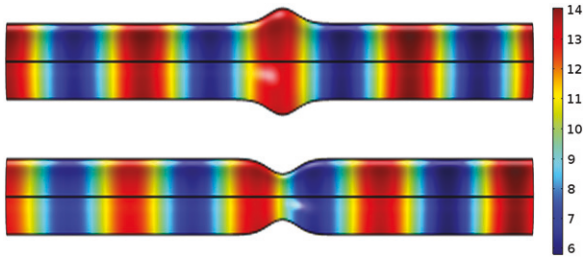

Fig. 1: Patterns from the Thomas-Murray RD model in eq. (6) are entrained to a Gaussian-shaped ridge, switching in phase between inward and outward deformations. Red (blue) indicates a high (low) concentration of chemicals. Vertical dimension magnified 3×. Parameters: $\nu_1 = 1$, $\nu_2 = 10$, $u_{10} = 92$, $u_{20} = 64$, $\alpha = 1.5$, $K = 0.1$, $\gamma = 2$, and $\rho = 18.5$. Unless specified otherwise, other figures have these parameters.

We used COMSOL Multiphysics® [36], which approximates the Laplacian by finite differences on a mesh and computes the fully nonlinear reaction terms. (See supplemental COMSOL models, `cylinder_gaussian_deformation.mph`, `deformed_sphere.mph`, `noise.mph`, `periodic-cylinder-length-sweep.mph`.) It should be noted that, although periodic boundary conditions are enforced in the numerical calculations, the computational methods using by COMSOL have a tendency to pin the resulting Turing patterns in a specific configuartion, even on a flat cylinder. Despite this, as shown in fig. 1, density maxima of Turing patterns on a deformed cylinder are entrained by a ridge. An inward (outward) ridge selects the sine (cosine) mode.

This conformal mapping approach enables studies of other geometries, including bumps on spheres (below), drums (see SM), and rippled cylinders. An axially symmetric rippled cylinder, $h(z) = \cos[(2\pi p/L)z] \equiv \cos(\bar{p}z)$, gives a Schrödinger-like equation at $\mathcal{O}(\epsilon)$ (cf. eq. (4)):

$$[-\Delta^0 - 2\epsilon\lambda_{sk}^{(0)}\cos(\bar{p}v)]\phi_k = k^2\phi_k. \tag{7}$$

This Schrödinger equation describes a particle moving in a weak periodic potential, whose properties are well understood in the context of solid-state physics [38]. At leading order, this perturbation gives rise to a broken degeneracy (band-gap) at $k = p/2$ with magnitude $4\epsilon\lambda_{sk}^{(0)}$. Our analysis predicts that when an RD system governs surface concentrations, the effective diffusion rate will increase in troughs and slow down on ridges. Hence, diffusion is enhanced (diminished) where Gaussian curvature is negative (positive). This agrees with the short-time analysis of diffusion on Riemannian manifolds, where the leading-order correction to diffusion is proportional to the Gaussian curvature [33–35]. For Turing patterns, steady-state regions of high concentration switch sharply from ridges to troughs as the most unstable wavelength is dialed past twice the ripple wavelength, see fig. 2 and supplementary video `rippled-cylinder.mov`. Note that eq. (7) predicts a broken degeneracy only when the most unstable

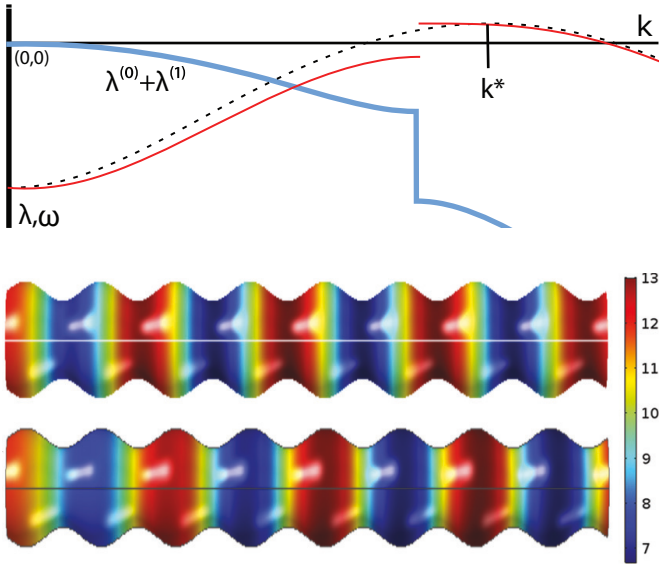

Fig. 2: Top: three functions of wave number: Laplacian eigenvalues on a rippled cylinder, including a band gap at $p/2$ (blue line); Turing spectrum on a nonrippled cylinder (black dotted line); Turing spectrum on a rippled cylinder (red line). For the case shown with $k^* > p/2$, the sine mode is selected; (cosine selected if $k^* < p/2$). Bottom line: numerical confirmation: concentration patterns in the Thomas-Murray model switch from troughs to ridges as the unstable chemical wavelength, k^*, is dialed past twice the ripple wavelength by changing $\gamma = 1.125$ (upper image) to $\gamma = 0.975$ (lower image). Vertical dimension magnified 3×. The SM includes a video of sweeping p (Mathematica and COMSOL files).

wavelength is commensurate with the ripple wavelength. However, in numerical simulations (presumably due to higher-order effects), we observe pinning for a range of wavelengths close to commensurability, although the patterns become unpinned for sufficiently incommensurate wavelengths.

An axially symmetric distorted sphere, described by $R(\theta)$, has line element

$$\mathrm{d}s^2 = \left(R^2 + R'^2\right)\mathrm{d}\theta^2 + R^2\sin^2\theta\mathrm{d}\varphi^2\,,$$

where the prime denotes derivatives. Mapping to conformally flat coordinates:

$$\mathrm{d}s^2 = \Omega^2\left(\mathrm{d}\Theta^2 + \sin^2\Theta\mathrm{d}\varphi^2\right).$$

The Laplacian eigenvalue equation in conformal coordinates becomes (see SM)

$$\left[-\Delta^0 + k^2\left(R_0^2 - R^2\frac{\sin^2\theta}{\sin^2\Theta}\right)\right]\Phi = k^2R_0^2\Phi\,, \tag{8}$$

where Δ^0 is the Laplacian on a round sphere. Setting $R = R_0\left(1 + \epsilon h(\theta)\right)$, we expand in powers of ϵ. To $\mathcal{O}(\epsilon)$, $\theta = \Theta$, and eq. (8) reduces to

$$\left[-\Delta^0 - 2\epsilon k^2R_0^2h\right]\Phi = k^2\Phi\,. \tag{9}$$

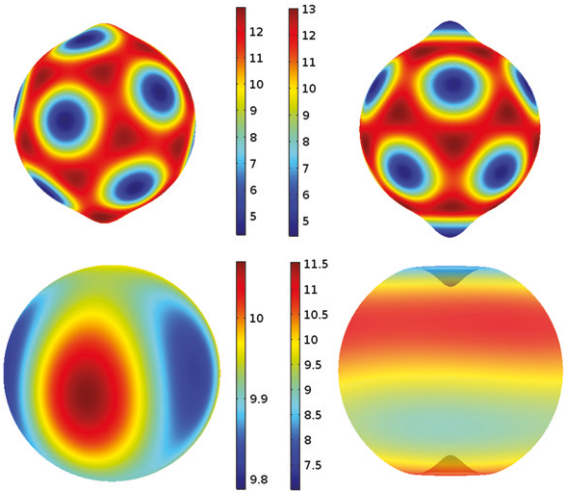

Fig. 3: Sufficiently large bumps entrain spotted patterns (top pair). Initial patterning on an undeformed sphere shows Y_5^5 (bottom left); the inward bumps of a "pinched sphere" amplify lower harmonics, causing Y_3^0 to appear (bottom right).

Using eq. (9), we study how deformations modify the Laplacian eigenfunctions $Y_\ell^m(\theta,\phi)$. The perturbation depends only on θ, breaking rotational symmetry by fixing polar orientation of eigenmodes while preserving azimuthal symmetry. This can potentially entrain Turing patterns, although there are competing influences from nonlinear effects and incommensurability of length scales as seen in fig. 3. In fact, in numerical simulations, we often found that the initial patterning predicted by linear stability analysis would stabilize to more complex patterns. In contrast, on a cylinder, initial patterning tends to persist indefinitely. We attribute this to differing degrees of degeneracy. The spherical eigenmodes, Y_ℓ^m, have $2\ell+1$ degeneracy. Thus, near the most unstable eigenmode, there are 2ℓ additional unstable modes that can contribute to nonlinear pattern formation. In contrast, a cylinder presents only a twofold degeneracy.

As evident from eq. (9), eigenfunction modifications are sensitive to the sign of h. An inward (outward) bump causes an increase (decrease) in diffusion. Nonlinear effects in the Thomas-Murray model are known to stabilize spotted patterns instead of the single most unstable spherical harmonic, see ref. [39]. However, during the initial development of Turing patterns, the most unstable Y_ℓ^m is visible, and the mode selected by a deformed sphere differs from that of a uniform sphere, see fig. 3.

Including extrinsic noise in RD systems leads to temporally fluctuating *quasi-patterns* for a broader range of parameters than those required for a Turing instability [11,16,40,41]. We have investigated how curvature influences such *noise-induced transient* patterns. We add uncorrelated white noise $\eta(\mathbf{x},t)$ of zero mean and variance $\mathcal{D}$ to eq. (5). In the linearly stable regime, this noise leads to eigenfunction fluctuations with a power spectrum $P(\lambda)$ proportional to $\mathcal{D}[\det\mathbf{M}(\lambda)]^{-1}$. On a uniform surface,

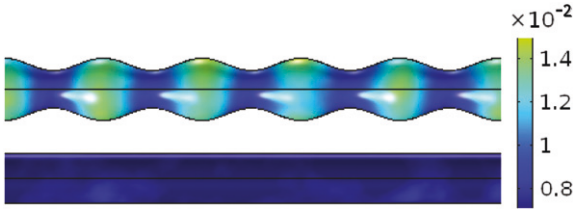

Fig. 4: Noise-induced quasipatterns appear when geometric ripples split degenerate eigenmodes of an RD system below threshold. Deformations pin the time-averaged intensity of fluctuations in RD quasipatterns (top); compare with the same intensity of extrinsic noise on a flat surface (bottom). For both panels, $\nu_2 = 6$ and $K = 0.15$.

time-averaged fluctuations are translationally invariant, $\langle\langle|\Psi(x)|^2\rangle = \Psi_0^2$. Deformations break this symmetry, leading to average fluctuations on a cylinder of the form

$$\langle|\Psi(x)|^2\rangle \propto \sum_k \frac{\cos^2(\bar{k}x)}{\det\mathbf{M}(\lambda_{0k}^+)} + \frac{\sin^2(\bar{k}x)}{\det\mathbf{M}(\lambda_{0k}^-)} + \mathcal{O}(\epsilon^2). \quad (10)$$

On spheres, the spherical harmonics replace the Fourier modes. Figure 4 shows numerical verification that such deformations fix the phase of fluctuations and create nonuniform time-averaged intensities. Such behavior is expected to hold generically for quasi-patterns induced by intrinsic noise [11,16,40,41], where the power spectrum describing fluctuations is qualitatively similar.

If these effects can be realized in manufactured or experimental systems, they could enable systematic manipulation of patterns. For example, collagen vitrigel (CV) for corneal endothelial regenerative treatment [42] could be molded in a hemispherical or eggcrate geometry and used to support zebrafish chromatophores, which were recently cultured for *in vitro* studies [14] to explore RD models [13]. Mice hair follicle patterning is also driven by an RD system involving WNT growth factor [43], and might be cultured on molded CV using established *in vitro* techniques [44]. Zebrafish stripes and hair follicles have spacing on the order of one hundred microns. Three orders of magnitude smaller, cytoskeletal suspensions exhibit patterns [3–5] that may realize our results. For example, a pinched sphere might be constructed in the recently studied encapsulations of actomyosin in giant unilamellar vesicles [6]. A recent review of such active fluids suggests that coupling to RD systems looks like a fruitful direction for research [7].

Even in a system as simple as a cylinder with a ridge, geometry can dramatically affect pattern formation. Our approach to the Laplacian on curved surfaces opens a new route to the analytical understanding of patterns in real systems, taking advantage of intuition and tools from quantum mechanics. Future directions include pattern formation in the presence of advection [8], and on time-varying shapes. Our approach can also be applied to scenarios involving interactions between the surface and boundary physics. In particular, it would be interesting to

examine the effect of nonuniform surface curvature when additional reaction-diffusion processes take place at the boundary [45]. More generally, our mathematical methods apply to any process described by the Laplacian, and may also find application in soap films [46], or Marangoni flows from surface tension gradients [47].

* * *

JRF acknowledges support from the Hertz Foundation. JG acknowledges support from CONACyT grant 180901. MK acknowledges support from DMR-1708280.

REFERENCES

[1] Turing A. M., *Philos. Trans. R. Soc. London, Ser. B, Biol. Sci.*, **237** (1952) 37.
[2] Hecht I., Kessler D. A. and Levine H., *Phys. Rev. Lett.*, **104** (2010) 158301.
[3] Bois J. S., Jülicher F. and Grill S. W., *Phys. Rev. Lett.*, **106** (2011) 028103.
[4] Giomi L. and Marchetti M. C., *Soft Matter*, **8** (2012) 129.
[5] Pearce D., Ellis P. W., Fernandez-Nieves A. and Giomi L., arXiv preprint, arXiv:1805.01455 (2018).
[6] Dürre K., Keber F. C., Bleicher P., Brauns F., Cyron C. J., Faix J. and Bausch A. R., *Nat. Commun.*, **9** (2018) 1630.
[7] Marchetti M. C., Joanny J.-F., Ramaswamy S., Liverpool T. B., Prost J., Rao M. and Simha R. A., *Rev. Mod. Phys.*, **85** (2013) 1143.
[8] Kumar K. V., Bois J. S., Jülicher F. and Grill S. W., *Phys. Rev. Lett.*, **112** (2014) 208101.
[9] Almarcha C., Trevelyan P. M., Grosfils P. and De Wit A., *Phys. Rev. Lett.*, **104** (2010) 044501.
[10] Murray J., *J. Theor. Biol.*, **88** (1981) 161.
[11] Butler T. and Goldenfeld N., *Phys. Rev. E*, **84** (2011) 011112.
[12] Kondo S. and Miura T., *Science*, **329** (2010) 1616.
[13] Nakamasu A., Takahashi G., Kanbe A. and Kondo S., *Proc. Natl. Acad. Sci. U.S.A.*, **106** (2009) 8429.
[14] Yamanaka H. and Kondo S., *Proc. Natl. Acad. Sci. U.S.A.*, **111** (2014) 1867.
[15] Sasai Y., *Nature*, **493** (2013) 318.
[16] Biancalani T., Jafarpour F. and Goldenfeld N., *Phys. Rev. Lett.*, **118** (2017) 018101.
[17] Corson F., Couturier L., Rouault H., Mazouni K. and Schweisguth F., *Science*, **356** (2017).
[18] Isaac E. B., Manor U., Kachar B., Yochelis A. and Gov N. S., *Phys. Rev. E*, **88** (2013) 022718.
[19] Turner A. M., Vitelli V. and Nelson D. R., *Rev. Mod. Phys.*, **82** (2010) 1301.
[20] Fialho A. R., Bernardino N. R., Silvestre N. M. and Telo da Gama M. M., *Phys. Rev. E*, **95** (2017) 012702.
[21] Shankar S., Bowick M. J. and Marchetti M. C., *Phys. Rev. X*, **7** (2017) 031039.
[22] Miller P. W., Stoop N. and Dunkel J., *Phys. Rev. Lett.*, **120** (2018) 268001.
[23] Thalmeier D., Halatek J. and Frey E., *Proc. Natl. Acad. Sci. U.S.A.*, **113** (2016) 548.
[24] Vandin G., Marenduzzo D., Goryachev A. B. and Orlandini E., *Soft Matter*, **12** (2016) 3888.
[25] Yu S., Wang H., Ni Y., He L., Huang M., Lin Y., Qian J. and Jiang H., *Soft Matter*, **13** (2017) 5970.
[26] Nampoothiri S., *Phys. Rev. E*, **94** (2016) 022403.
[27] Sánchez-Garduño F., Krause A. L., Castillo J. A. and Padilla P., to be published in *J. Theor. Biol.* (2018).
[28] Nampoothiri S. and Medhi A., arXiv preprint, arXiv:1705.02119 [cond-mat.soft] (2017).
[29] Kac M., *Am. Math. Mon.*, **73** (1966) 1.
[30] Schoen R. and Yau S., *Lectures on Differential Geometry*, *Conference Proceedings and Lecture Notes in Geometry and Topology* (International Press) 1994.
[31] Rosenberg S., *The Laplacian on a Riemannian Manifold: An Introduction to Analysis on Manifolds*, *London Mathematical Society Student Texts* (Cambridge University Press) 1997.
[32] Braun V., Brelidze T., Douglas M. R. and Ovrut B. A., *JHEP*, **05** (2008) 080.
[33] David F., in *5th Jerusalem Winter School for Theoretical Physics*, 1987, pp. 157–223.
[34] Faraudo J., *J. Chem. Phys.*, **116** (2002) 5831.
[35] Castro-Villarreal P., *J. Stat. Mech.: Theory Exp.*, **2010** (2010) P08006.
[36] COMSOL, *Multiphysics v5.2a*.
[37] da Costa R. C. T., *Phys. Rev. A*, **23** (1981) 1982.
[38] Kittel C., *Introduction to Solid State Physics* (John Wiley & Sons) 2004.
[39] Barrio R. A., Varea C., Aragón J. L. and Maini P. K., *Bull. Math. Biol.*, **61** (1999) 483.
[40] Lugo C. A. and McKane A. J., *Phys. Rev. E*, **78** (2008) 051911.
[41] Schumacher L. J., Woolley T. E. and Baker R. E., *Phys. Rev. E*, **87** (2013) 042719.
[42] Yoshida J., Oshikata-Miyazaki A., Yokoo S., Yamagami S., Takezawa T. and Amano S., *Investigative Ophthalmol. Visual Sci.*, **55** (2014) 4975.
[43] Sick S., Reinker S., Timmer J. and Schlake T., *Science*, **314** (2006) 1447.
[44] Philpott M. P., Green M. R. and Kealey T., *J. Cell Sci.*, **97** (1990) 463.
[45] Halatek J. and Frey E., *Cell Rep.*, **1** (2012) 741.
[46] Osserman R., *A Survey of Minimal Surfaces* (Dover Publications) 2002.
[47] Pereira A., Trevelyan P. M. J., Thiele U. and Kalliadasis S., *Phys. Fluids*, **19** (2007) 112102.